

Sub-Module Integrated Distributed Maximum Power Point Tracking for Solar Photovoltaic Applications

Robert C.N. Pilawa-Podgurski
 UNIVERSITY OF ILLINOIS AT URBANA-CHAMPAIGN
 URBANA, ILLINOIS
 EMAIL: pilawa@illinois.edu

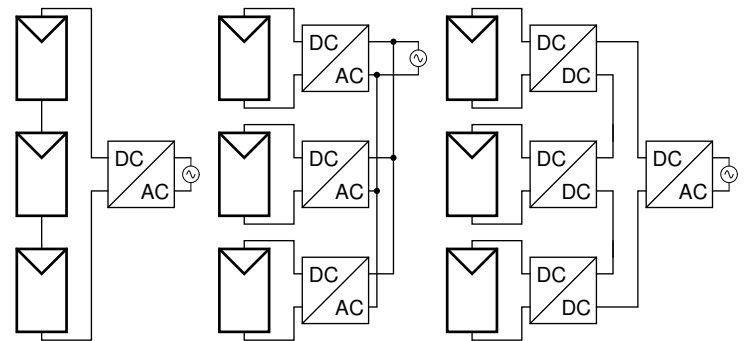
David J. Perreault
 MASSACHUSETTS INSTITUTE OF TECHNOLOGY
 CAMBRIDGE, MASSACHUSETTS

Abstract—This paper explores the benefits of distributed power electronics in solar photovoltaic applications through the use of sub-module integrated maximum power point trackers (MPPT). We propose a system architecture that provides a substantial increase in captured energy during partial shading conditions, while at the same time enabling significant overall cost reductions. This is achieved through direct integration of miniature MPPT power converters into existing junction boxes. We describe the design and implementation of a high-efficiency (>98%) synchronous buck MPPT converter, along with digital control techniques that ensure both local and global maximum power extraction. Through detailed experimental measurements under real-world conditions, we verify the increase in energy capture and quantify the benefits of the architecture.

I. INTRODUCTION

With rising world-wide energy demands and soaring prices of fossil fuels, interest in renewable energy sources has increased. Among these, solar photovoltaic (PV) energy has seen a rapid growth in the last few years, resulting in decreased prices of PV modules as production capacity increases at a fast pace. As PV module prices decrease, the cost of the power electronics required to extract the maximum power from the PV modules and to interface the PV system to the grid is becoming a larger part of the overall system cost [1]. Much attention has therefore been given to the development of power electronics that enable a cost reduction of the overall system. In addition, much research is focused on increasing the efficiency of the power processing stage, as well as on improving the power yield of the overall system [2], [3].

Many PV installations suffer from current mismatch between different modules, due to non-uniform shading of the array, dirt accumulation, or manufacturing variability. Ensuring uniform illumination is particularly challenging in residential PV applications, where large current mismatch can be present due to external objects that cause shading. Shown in Fig. 1(a) is the most common solar PV architecture, which connects all modules in series. In this architecture, any partial shading or other source of cell current mismatch will cause the overall system output power to be reduced, since the current in the string is limited by the weakest module. While modules used today typically employ bypass diodes that help protect the modules and limit the negative effect of partial shading, it is still the case that partial shading has a significant negative effect on any solar installation.



(a) Series string architecture. (b) Micro-inverter architecture. (c) Cascaded dc-dc (dc-dc optimizer) architecture.

Fig. 1. Schematic drawings of three kinds of distributed MPPT architectures for solar PV.

The micro-inverter (also known as module-level inverter or AC-Module) concept shown in Fig. 1(b) has been exploited to address this problem by operating each module at its unique maximum power point, and providing separate dc to ac conversion for each module. Using this architecture, any shading of a single module only affects its output power, without limiting the performance of the other modules in the installation. While the micro-inverter architecture can increase overall energy capture in a system, micro-inverters typically suffer from lower overall efficiency than high-voltage string-level inverters, owing to the large voltage transformation required to interface the module voltage (e.g. 20-40 Vdc) to the grid (e.g. 120-240 Vac rms), and often suffer from relatively high cost.

Recently, the concept of cascaded dc-dc converters (dc-dc optimizers) has become popular [4]–[6], where each PV module employs a dc-dc converter that performs maximum power point tracking (MPPT), and the output of the converters are connected in series. This architecture is shown in Fig. 1(c). Through dc-dc optimizers, localized control of module voltage and current can be achieved, and each module can operate at its independent maximum power point (MPP), thus improving the energy extraction of the overall system. The series connection of the outputs provides an inherent voltage stacking that enables each dc-dc converter to operate at a relatively low voltage conversion ratio (enabling high conversion efficiency),

while still achieving high overall output voltage, which is desirable as it enables the use of a central, high-voltage, high-efficiency inverter.

To date, however, the promise of dc-dc optimizers has not been fully realized, primarily due to the difficulty of simultaneously achieving high conversion efficiency *and* low cost of the power electronics. Low dc-dc conversion efficiency can easily negate any increase in energy capture that is offered by more localized (module-level) control, and must therefore be addressed. It should be mentioned that it is not merely the efficiency of the power electronics that must be addressed, but also how much of the available power that is extracted. Some circuit architectures, such as switched capacitor circuits [7], [8] provide very high efficiency and density, but cannot operate efficiently at arbitrary conversion ratios, thereby limiting maximum energy extraction. A goal is thus to achieve very high conversion efficiency in the power electronics, *as well as* high tracking efficiency (a measure of how close to the true MPP the module is operated).

Furthermore, a solution that increases total energy capture by a few percent, but which also increases the overall cost by more than the monetary value of the increased power (as compared to the installed system cost) will likely fail in the marketplace. In this paper, we present a dc-dc optimizer system that achieves both low cost and high conversion efficiency, while at the same time capturing substantially *more* energy than dc-dc optimizer architectures presented to date. In addition, detailed field experiments are presented that illustrate the benefits of our architecture under real-world partial shading conditions.

This paper is organized as follows: Our proposed system is presented in Section II, and Section III provides implementation details of the power converter designed for our architecture. The control implementation is discussed in Section IV, and experimental results and analysis are provided in Section V. A quantitative comparison to previous work is presented in Section VI, where we also introduce a Figure-of-Merit that incorporates cost, efficiency, and increase in energy capture. Finally, Section VII concludes the paper.

II. PROPOSED ARCHITECTURE

Dc-dc optimizer systems can be implemented with many different circuit topologies. Previous work at the module-level has employed boost converters [5] and non-inverting buck-boost converters [6]. While boost converters are an attractive option because of their ability to increase the output voltage (requiring fewer modules for a given desired output voltage), their chief disadvantage is their limited operating range. As discussed in [5], since the output current of a boost converter can never be higher than its input current, the range over which current mismatch can be addressed is severely limited. The non-inverting buck-boost converter is employed in [6], and can provide an output current that is both higher and lower than the input current, thus providing both a voltage increase and the ability to handle shaded modules (although within a limited range, since each converter only operates in

buck or boost mode at a given time). The chief disadvantages of the non-inverting buck-boost topology are the increased number of transistors and the achievable conversion efficiency, which is typically lower than buck or boost converters for the same switch rating. A more detailed performance analysis of a number of potential power converter topologies for dc-dc optimizers can be found in [9].

In this work, we implement the dc-dc optimizer system using synchronous buck converters. While the synchronous buck topology enables both high switching frequency (important for small size and low cost) and high efficiency, it does not contribute any voltage gain (which would reduce the number of modules that must be series connected). In most residential and utility-based installations, however, there are a sufficient number of PV modules to provide for the inherent stacking of voltages without requiring additional step-up from the power converter. When not tasked with providing additional voltage step-up, the power stage can be optimized for size, cost, and efficiency. As our experimental results indicate, the synchronous buck converter topology offers size, cost, and efficiency benefits, and the system can be operated in a manner where the control implementation is relatively simple. Meanwhile, the string current can be kept sufficiently low so that the added wiring conduction losses are kept to a minimum.

In order to increase the overall system energy capture, our design employs sub-module distributed MPPTs, as shown in Fig. 2¹. Using this architecture, mismatch between different sub-modules within the same module can be mitigated, which yields an increase in energy capture compared to module-level MPPTs. Furthermore, each MPPT in Fig. 2 only sees a third of the module voltage, and can thus be designed using components with lower voltage rating than module-level MPPTs. The use of low-voltage power MOSFETs with their small parasitics in turn enables an increase in achievable switching frequency, which enables reduced passive component size and cost. As will be shown in Section III, it is even possible to miniaturize the MPPTs to the point where they can fit in the existing standard junction box at the back of the PV module. This leads to further cost reductions, as a large custom outdoor-rated enclosure contributes significant cost to a dc-dc optimizer system.

III. SUB-MODULE DISTRIBUTED MPPT CONVERTER

The inset of Fig. 2 shows a schematic drawing of the sub-module MPPT system designed as part of this work. The system comprises a synchronous buck converter power stage controlled by a microcontroller to achieve local MPP operation. The microcontroller can sense voltage, and also employs lossless current sensing [10] for control algorithms that also require current information. Each converter employs an isolated I2C communication interface, enabling bidirectional information transfer to a master node, which can be a

¹We will refer to all cells in a PV module that are connected to the same bypass diode as a sub-module. The most common type of PV modules comprise three sub-modules.

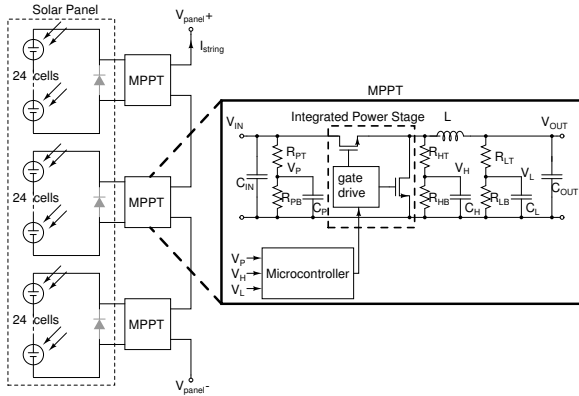


Fig. 2. Schematic drawing of the sub-module integrated MPPT system. A component listing is provided in Table I.

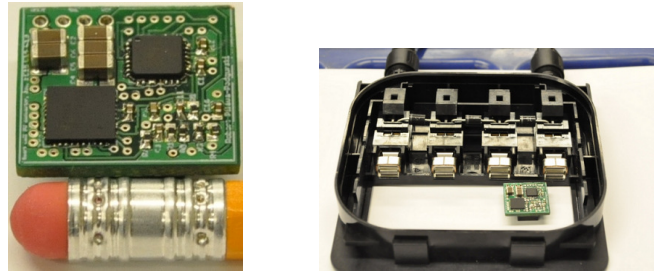
TABLE I
COMPONENT LISTING

Device	Model	Value	Manufacturer
Integrated Power Stage	FDMF6704A		Fairchild
L	SER1360-103KL	10 μ H	Coilcraft
R_{HT}, R_{LT}, R_{PT}	0402	100k Ω	Panasonic
R_{HB}, R_{LB}, R_{PB}	0402	10k Ω	Panasonic
C_H, C_L, C_P	0402	1 μ F	Murata
C_{IN}	1206, X5R, 25V	3 x 10 μ F	Murata
C_{OUT}	1206, X5R, 25V	2 x 10 μ F	Murata
Microcontroller	ATtiny861		Atmel

dedicated microcontroller or a computer. It should be noted that each MPPT can operate without any communication interface, but the I2C interface is used here to gather diagnostic data from each converter, and to provide a simple means for controlling the global output power. Table I provides a listing of the components used in the design. A complete bill-of-material and cost analysis can be found in [9].

Shown in Fig. 3(a) is a photograph of the complete converter prototype, together with a pencil for scale; the overall converter “box volume” is 4 cm³. Shown in Fig. 3(b) is one of the MPPTs placed in a typical solar module junction box. In a full installation, three converters are used per PV module, one in parallel with each bypass diode. It is evident from the photograph that three converters fit in the junction box, with plenty of space for connectors and sufficient air flow for passive cooling. A goal of the power stage design was to achieve a small enough converter footprint to fit into the junction box on the back of off-the-shelf PV modules. By utilizing the existing weather-resistant junction box as an enclosure, significant cost savings can be realized. The Integrated Power Stage is a combined gate-drive and power MOSFET chip (FDMF6704A), which also incorporates a 5 V linear regulator, enabling the converter to be completely powered from the sub-module cell stack.

In order for the sub-module distributed MPPT architecture of Fig. 2 to be effective, it is important that the additional



(a) Photograph of the sub-module MPPT converter, with a pencil shown for scale. The power inductor is on the bottom side of the PCB.

(b) Photograph showing the sub-module MPPT together with a solar module junction box. The three bypass diodes are also visible; an MPPT converters is placed in parallel with each diode.

Fig. 3. Photographs of sub-module MPPT hardware.

TABLE II
CONVERTER SPECIFICATIONS

Input Voltage Range	5-27 V
Output Voltage Range	0.8-20
Max Output Power	80 W
Switching Frequency	250 kHz
Converter Peak Efficiency	98.2%

power captured is not wasted by low conversion efficiency of the power electronics. Much care was thus taken in this work to achieve high efficiency operation, both through the choice of topology and passive components, as well as the implementation of sensing and control. A detailed description of these efforts can be found in [9]. Shown in Table II is an overview of the specifications of the converter, along with a performance summary.

A detailed efficiency and power characterization of the MPPT converter has been carried out to measure performance across a wide load and output voltage range. Fig. 4 shows a plot of efficiency versus output voltage, parameterized by output current, for a fixed input voltage of 12 V. No attempts were made in this design to provide increased light-load efficiency, but we note that in general, this can be accomplished with suitable light-load control scheme, such as pulse-frequency modulation (PFM), if desired. The converter will operate at lower output voltages if it suffers from more shading relative to the other converters in the string. A low output current would signify that the insolation of the entire string of MPPTs is relatively low.

Given these characteristics of the system, it is important to achieve high efficiency at high power levels (for maximum total energy capture), as well as at operating points where the converter is expected to spend significant time in real-world scenarios. In Fig. 4, this would correspond to high output voltage (no or little shading) and high current (>5 A, corresponding to high insolation). We see from the plot that we achieve an efficiency above 97% under these conditions. The peak efficiency of 98.2% is realized at an input voltage of 16 V, and an output current of 5 A. It should be noted

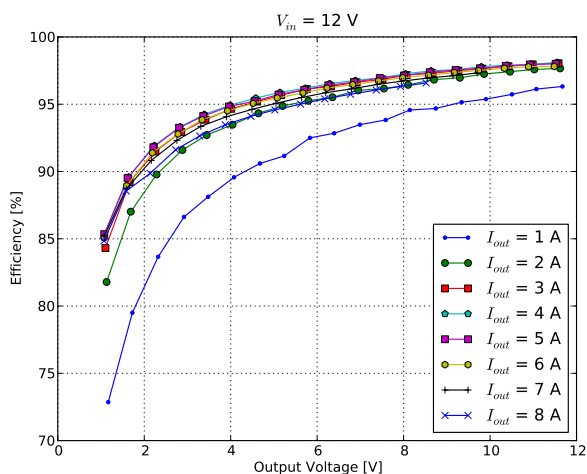


Fig. 4. Measured efficiency versus output voltage, parameterized by output current. A lower output voltage corresponds to a shaded sub-module, while a lower output current signifies a string with less insolation.

that all efficiency measurements include all sensing, gate drive and control losses, as the converter itself is powered from its input terminals. A more detailed performance characterization of the power stage across a variety of operating conditions can be found in [9]; excellent efficiency is maintained across an input range from 8-16 V, and the converter functions over a still much wider range.

IV. CONTROL IMPLEMENTATION

In our architecture, owing to the sub-module integrated dc-dc converters, there are no local maxima in the I-V characteristics of the overall system (these are caused by conducting bypass diodes in regular PV modules during partial shading). In order to extract maximum energy from a PV installation with sub-module power tracking, each MPPT must continuously operate its sub-module at the correct current and voltage, while also allowing all other MPPTs do the same for their individual sub-modules. We must thus design a control algorithm that ensures that each sub-module operates at its *local* MPP, while also ensuring that the overall system operates at the *global* MPP (i.e., the overall string voltage and current are such that all sub-modules are operating at their respective MPPs).

A. Local MPPT algorithm

Since the outputs of the individual power trackers are connected in series (as seen in Fig. 2), all of them share the same output current (I_{string}). Each converter can thus maximize its own output power by maximizing its output voltage. It thus follows that a local MPPT algorithm can be implemented by driving the local output voltage to its maximum value. In our implementation, we employ a Perturb and Observe (P & O) algorithm that continuously tracks the MPP by making small changes to the duty cycle in order to drive the converter output voltage to its maximum.

TABLE III
MPPT TRACKING PARAMETERS

MPPT Duty Cycle Step-Size	0.6%
MPPT Startup Sweep Step-Size	5%
Minimum Duty Cycle	10%
Maximum Duty Cycle	99 %
ADC Resolution	10 bit
ADC Samples Per Measurement (Overampling)	100

In order to quickly locate the approximate location of the MPP, the converter starts by performing a coarse sweep of its duty cycle, and measuring the corresponding values of output voltage. The duty cycle corresponding to the maximum voltage observed is recorded, and at the end of the startup sweep the converter is set to operate at this duty cycle. At this point, the steady-state tracking algorithm begins, which uses a perturb and observe algorithm which aims to maximize the converter output voltage by making small changes (ΔD) to the duty cycle (D). In this manner, the sub-module MPPT will continuously track the MPP, and oscillate around it to within the finite precision of its voltage sensing and duty cycle control. The MPPT P & O rate used in our experiments was 10 Hz. It should be pointed out that this rate was limited by the I2C communication bandwidth. The delay between each time-step was caused by each converter communicating its input and output voltage, as well as duty cycle to the computer for data analysis. The microcontroller itself is capable of operating at an MPPT rate in excess of 25 kHz, which is significantly faster than what is required for this application. Table III provides information about our sensing and PWM resolution and step-size for the experimental prototype.

B. Global MPPT algorithm

By adjusting the duty ratio, the local MPPT can autonomously achieve MPP operation so long as the sub-module current at its MPP is equal to or less than that of the string².

To achieve global MPP operation, each sub-module controller adjusts its duty ratio for MPP operation (e.g., in a “fast” loop) based on the string current, while the system level controller (typically implemented by the grid-interface inverter) adjusts the string current (in a “slow” loop) such that there is just sufficient string current available for the sub-module with the highest MPP current. In this manner, the control problem can be separated into a local MPPT control for each sub-module, along with a single global control loop that only requires limited information.

1) *1-bit Feedback Global Algorithm*: A method to ensure that the overall system is operating at the global MPP is to signal to the global (“slow”) loop controller when one of the local MPPTs is operating at or near its maximum permitted duty cycle. At this point, the system loop controller may

²This constraint is due to the chosen power converter topology (buck converter), which can only provide an output current greater than or equal to the input current.

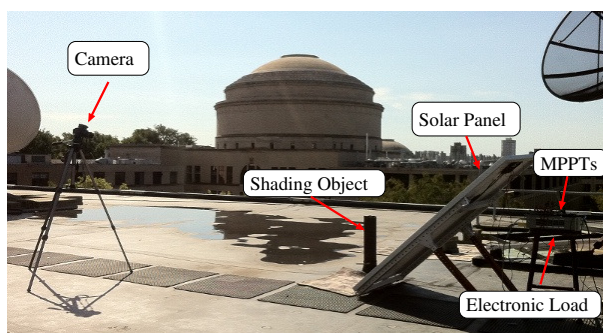


Fig. 5. Annotated photograph of the field experiment setup.

not decrease the current (I_{string}) any further, as the strongest MPPT would then not be operating at its MPP. This 1-bit feedback signal can be implemented either using a very simple single-interconnect or zero-interconnect communications link, or by encoding the information to communicate it directly via the series string interconnect. (We note that such methods are well known in other types of distributed power conversion systems [11], [12] and can be implemented without significant expense in this application.)

We note that the architecture presented here also makes possible the use of a global MPPT algorithm requiring no communication between the local and global controller, as presented in [9]. For the experimental measurements shown here, we implemented the 1-bit feedback algorithm, so we do not further elaborate on the communication-less global MPPT algorithm here. Interested readers are referred to [9].

V. FIELD MEASUREMENT EXPERIMENTAL RESULTS

In order to fully evaluate the distributed MPPT system in a real setting, we chose to perform outdoor field experiments under a variety of conditions. A PV module with three internal sub-modules (the STP175S-24/Ab01 72-cell monocrystalline Si module from Suntech) was mounted in a south-facing direction together with test equipment on a flat roof of a building on the MIT campus. Figure 5 shows an annotated photograph of the field setup. The camera was used to produce time-lapse photos of the shading pattern of the module. The photos were synchronized with the output power measurement, providing a visual check to discern shading patterns related to module I-V characteristics. The distributed MPPTs were connected across each sub-module (in parallel with the existing junction diodes, as shown in Fig. 2), and their output connected to an electronic load (HP6060B). The electronic load was controlled through the GPIB interface by a small netbook computer that recorded all data.

To effectively characterize the performance benefit of the sub-module distributed power electronics compared to a conventional solar module, a low on-state resistance bypass MOSFET (PSMN8R5-60YS by NXP) was used for each sub-module, such that the system could be alternated between employing distributed MPPT (MPPTs on, bypass MOSFETs off), and conventional operation (MPPTs off, bypass MOSFETs

on).

A. Static Performance Evaluation

Our first experiment was to evaluate the relative performance improvement offered by the distributed MPPT during a static sub-module mismatch scenario. In this case, we performed measurements with and without distributed MPPT for a module where a single cell experienced various degrees of shading. This scenario is representative of static mismatch caused by for example dirt accumulation, bird droppings, a damaged cell, or a severe local degradation of the module encapsulant.

Shown in Fig. 6 is a plot of measured module output power versus load current when a single cell in the module is shaded by 50%, under constant outdoor insolation (i.e. a short measurement on a cloud-free day). The solid blue line represents the measurement with the module connected directly to the electronic load, without distributed MPPTs. In this case, the electronic load was first connected to each individual sub-module, to generate a plot of power versus output current. It can be clearly seen that sub-module 3 has a lower maximum output current (and hence power) due to the single shaded cell in that sub-module.

Furthermore, from the plot showing the full module power without distributed MPPT, two maximum power points can be seen. This is due to the bypass diode connected to sub-module 3 conducting when the electronic load is drawing more current than the maximum current available from sub-module 3. In this case, it can be seen that the global maximum power point is the case where the bypass diode is not conducting, whereas the other point is a local maximum power point. Situations like this present problems for the MPPT algorithms in both centralized inverters and micro-inverters, as they can easily get stuck on the local maximum power point. Table III provides the MPPT tracking parameters used for this and all subsequent MPPT tests. The minimum achievable duty cycle step-size with the hardware we implemented was 0.1%, but the 0.6% step-size provided a good trade-off between conversion speed and steady-state accuracy.

The circles in Fig. 6 represent discrete data points collected with the distributed MPPT converters enabled, for a variety of output currents (stepped by the electronic load). In this measurement, the electronic load stepped the output current to the indicated values with enough time (a few seconds) between steps to ensure that the distributed MPPTs reached their steady-state points after each step. For this shading scenario (a single cell shaded by 50%), a 24% increase in achievable power output can be observed. The increase in power output is of course dependent on the particular shading pattern (we have measured instances of more than 30% increase in output power for certain shading patterns). Furthermore, the module with integrated sub-module MPPTs produces close to its maximum power across a broad range of output currents. In a complete system with a central inverter, this characteristic would enable the inverter to extract maximum power over a wide voltage

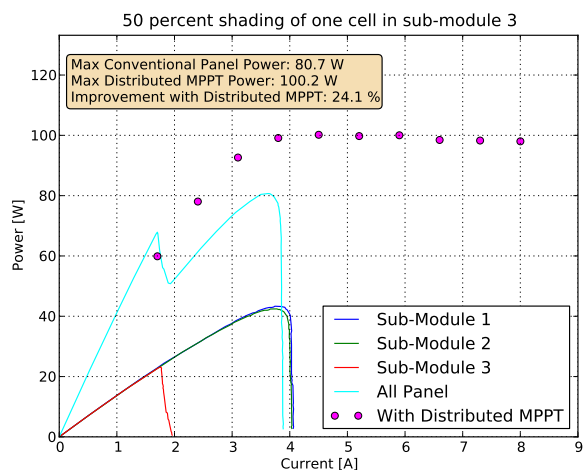


Fig. 6. Plot of power versus current with and without distributed MPPT, for 50% shading of one cell in sub-module 3. A power increase of 24% is obtained by the use of the sub-module MPPTs. This data was taken at MIT on October 6th, 2011, which was a very sunny day with no cloud coverage.

TABLE IV
STATIC SHADING PERFORMANCE

Shading of single cell	Module power without sub-module MPPT	Module power with sub-module MPPT	Change
75 %	75.2 W	83.5 W	+11.0%
50 %	80.7 W	100.2 W	+24.1%
25 %	103.4 W	115.1 W	+11.3%
0 %	135.5 W	132.4 W	-2.3 %

and current range, rather than the single point associated with a conventional PV system.

We have performed a number of measurements on different static scenarios, details of which can be found in [9]. Table IV summarizes these results, where the relative improvement of the distributed MPPT architecture can be clearly seen. For a perfectly matched module with no shading throughout the day, however, our proposed system would not be beneficial, as seen from the decrease in output power when employing the distributed MPPT for 0% shading of a single cell. This should come as no surprise, as any added power electronics incur some loss, and if there is no inherent mismatch in the module, there is nothing to be gained from employing additional MPPTs. It should be pointed out, however, that it is fairly trivial to implement a bypass-mode in the MPPTs themselves, such that during times of no shading the MPPTs are bypassed altogether, and thus are not contributing any loss. This bypass-mode can be implemented in firmware only (turning the top MOSFET on permanently, with some additional conduction loss in the switch and inductor), or with one additional bypass MOSFET with low on-state resistance (this approach will give the lowest loss in no-shading situations).

B. Dynamic Performance Evaluation

To evaluate the performance of the sub-module distributed MPPT architecture under dynamic partial shading conditions,



Fig. 7. Photograph illustrating the shading (owing to a protruding pipe) that moves across the module for the dynamic performance experiment.

we performed the following field experiment under practical real-world conditions:

The module was placed near a metal chimney (visible in Fig. 5), so that only a small number of cells were shaded, as illustrated in Fig. 7. As the sun moves throughout the day, the location of the shadow on the module moves as well, covering different sections of the module to varying degrees. This situation is very similar to what would happen in residential installations, where chimneys, power lines, trees, antennas, and other structures block parts of the module throughout the day.

The system was set up such that approximately every minute it would switch between bypassing the distributed MPPTs, and connecting them to the module. When the MPPTs are bypassed (i.e. the module is configured just like a conventional module) the electronic load performs a full I-V sweep of the module, and the highest power is recorded. When the MPPTs are connected, the electronic load starts at a current (6 A) that is higher than the module short-circuit current (5.2 A), and waits for the MPPT outputs to reach steady-state (a few seconds). It then decreases the current, at each time waiting for the MPPTs to settle again. It continues to decrease the current until one of the MPPTs (the one connected to the strongest sub-module) reaches its maximum allowed duty cycle (0.99). At this time any further decreases in module output current will mean that at least one of the MPPTs is not operating at the sub-module MPP, so the sweep is stopped, and the highest output power recorded. This effectively reflects operation with the one-bit feedback global MPPT algorithm described in Section IV.

Shown in Fig. 8 is a plot of module output power versus time, with and without the distributed MPPT electronics active, as discussed above. These measurements were taken on a very sunny day (Oct 6, 2011) at the times indicated in the plot. It can be seen that at all times during the measurement period, the distributed MPPT system generated more power from the module than what a conventional module would generate, thanks to the mitigation of sub-module current mismatch owing to partial shading.

Shown in Fig. 9 is the accumulated energy extracted from the module during the measurement time, and it shows that

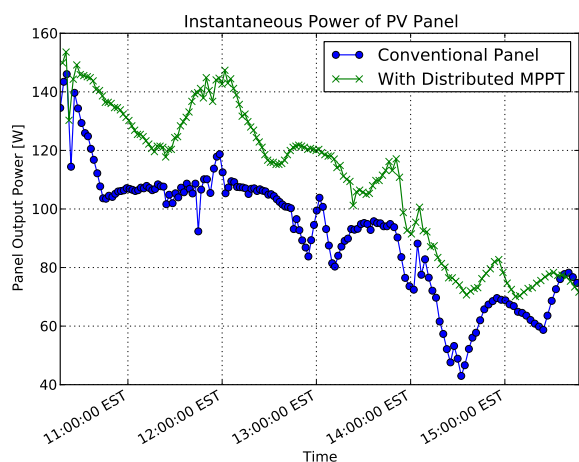


Fig. 8. Instantaneous measured power versus time for a sunny day (October 6, 2011) for a conventional module, as well as with the distributed MPPT employed, for the test setup illustrated in Fig. 5. Up to a 30% increase in captured power is observed.

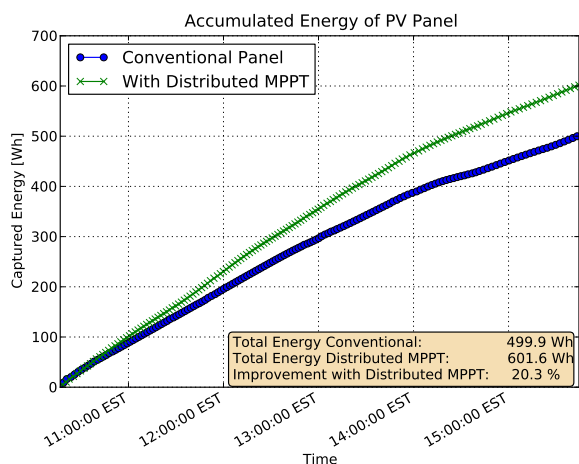


Fig. 9. Accumulated energy versus time for a sunny day (October 6, 2011) for a conventional module, as well as with the distributed MPPT employed. The distributed MPPT system collects more than 20% additional energy over a conventional module.

the distributed MPPT system collected over 20% more energy over the course of this experiment than what a conventional module would achieve.

VI. PERFORMANCE COMPARISON

The previous section illustrates the improvements in overall power and energy capture that can be realized with the use of the sub-module MPPT architecture and the hardware implemented in this work. In solar PV applications, which are very cost sensitive, it is illustrative to perform a cost analysis to quantify the cost-benefit trade-off of this increase in power. A small increase in output power that comes at a large added system cost is clearly not worthwhile, and in this section we provide a quantitative analysis of this trade-off, based on the

empirical data captured in our experiment.

Shown in Table V is a comparative chart of our work, previous academic work, as well as two selected commercial solutions. The topology, cost, power density, efficiency, and a figure of merit (discussed below) are listed. For the academic work, we have attempted to estimate the complete converter cost from published results³ (the commercial prices are estimates from reported retail prices), and adjusted the efficiencies so that they each include all control and gate driver losses for a fair comparison. It should be noted that aside from the work presented here, none of the other solutions provide sub-module tracking, and thus only address mismatch at the panel level. As was shown in the experimental section, sub-module mismatch can contribute to significant energy loss (up to 20%), which cannot be mitigated by the other solutions. We find that both in terms of efficiency and cost, our solution compares favorably to previously published work in the field, while also offering a significant increase in overall energy capture during partial shading conditions.

A. Figure of Merit

The merits of distributed MPPT in any solar PV system is entirely dependent of the particular installation. Some installations may benefit greatly from added power electronics, whereas others may see no improvement in overall energy capture (e.g., perfectly matched panels on a completely flat surface with no external objects that can cause shading). Due to the very site-specific circumstances, it is therefore difficult to quantify exactly how much a typical residential installation may benefit from our approach. It is, however, possible to quantify the relative merits of the power electronic solution itself, compared to other similar solutions. This is done in Table V, where we have introduced a figure of merit that aims to capture some of the cost/benefit trade-off with this approach. It should be pointed out that this figure of merit is a crude estimate of the relative performance between different solutions, and it should not be used as an absolute metric to judge whether distributed MPPT will pay off or not.

The figure of merit attempts to capture the incremental cost for the added average power to the PV system (given as \$/Watt). It calculates the expected additional average power captured by the system (accounting for the electrical conversion losses of the MPPTs in each case), for a given nominal power increase factor (α). This increase factor represents the fractional increase in average output power that can be expected with the distributed MPPT system, and as such, is highly installation dependent. For our analysis, an α of 0.1 is chosen for per-panel MPPT, and 0.15 for sub-module MPPT (this is a modest 5% increase for sub-module MPPT compared to per-panel MPPT, keeping in mind that we experimentally measured between a 10% and 20% increase in captured energy for the sub-module case versus regular panel-based MPPT in our field experiments). The Figure of Merit is given by:

³Note that the cost presented in [6] does not include the cost of the micro-controller, gate-driver, auxiliary power supply, and many other components. They are added into the cost used here to provide a fair comparison.

TABLE V
DC-DC OPTIMIZER PERFORMANCE COMPARISON

Work	[6]	[5]	[13]	National	Azuray	This work
Type	Academic	Academic	Academic	Commercial	Commercial	Academic
Topology	Buck-Boost	Boost	Buck-Boost	Unknown	Unknown	Buck
Sub-Module Tracking	No	No	No	No	No	Yes
Volume [cm ³]	255 cm ³	unknown (big)	850 cm ³	680 cm ³	740 cm ³	12 cm ³
Cost	\$27	unknown (high)	\$65	\$150	\$90	\$12.80
Power [W]	85 W	60 W	100 W	230 W	300 W	200 W
Cost/Power [\$/W]	0.32 \$/W	high	0.65 \$/W	0.65 \$/W	0.3 \$/W	0.064 \$/W
Efficiency [%]	95%	93%	95%	98.5%	97.6%	98.2%
FOM [\$/W]	7.06 \$/W		14.44 \$/W	7.81 \$/W	4.07 \$/W	0.50 \$/W

$$FOM = \frac{\text{cost}}{\langle P_{\text{added}} \rangle}, \quad (1)$$

where P_{added} is the *additional* power captured owing to the power electronics:

$$\langle P_{\text{added}} \rangle = \eta_{MPPT} P_{\text{rated}} (1 + \alpha) - P_{\text{rated}}, \quad (2)$$

and η_{MPPT} is the electrical conversion efficiency of the MPPTs, and P_{rated} is the rated power of the MPPT. The FOM should be compared to the typical installed cost of solar PV systems, which was estimated to be around \$6/W in 2010 [14], but is rapidly decreasing. In order for the distributed MPPT system to be cost effective, the FOM must be below the installed cost of the PV system, for a given installation. We see that for our assumptions of a 10% and 15% total improvement in average power due to module and sub-module tracking, respectively, the cost benefit of many of the solutions of Table V are marginal. As the installed cost of solar PV continues to decrease, even further price pressure on the power electronics is expected. In light of this, our calculated FOM of 0.50 \$/Watt makes our solution cost competitive today, and for some time in the future.

VII. CONCLUSIONS

We have presented a sub-module distributed MPPT architecture for solar PV applications, which enables more energy to be extracted from the system. By employing low-voltage synchronous buck converters connected across each sub-module of the panel, a high frequency, very high efficiency power stage can be used. The power electronics can then be miniaturized to the point where they fit into the existing junction box, thereby greatly reducing cost. We have presented a hardware prototype for use in sub-module tracking of a PV panel, and discuss local and global control techniques to maximize the overall energy capture of the system. We measure up to a 20% improvement in overall energy capture compared to per-panel MPPT implementation, using field experiments with a partial shading obstacle, and perform static mismatch measurements that further validate the performance of the system. Finally, we compare our implementation to other, state-of-the-art commercial and academic solutions, and find

that the proposed solution offers attractive benefits in terms of efficiency and cost, both of which are critical in PV systems.

REFERENCES

- [1] "Trends in photovoltaic applications. survey report of selected IEA countries between 1992 and 2006," Tech. Rep. IEA-PVPS T1-16:2007, International Energy Agency Photovoltaic Power Systems, 2007. [Online] www.iea-pvps.org.
- [2] S. Kjaer, J. Pedersen, and F. Blaabjerg, "A review of single-phase grid-connected inverters for photovoltaic modules," *IEEE Transactions on Industry Applications*, vol. 41, no. 5, pp. 1292–1306, 2005.
- [3] J. Myrzik and M. Calais, "String and module integrated inverters for single-phase grid connected photovoltaic systems - a review," in *Proc. IEEE Bologna Power Tech Conference*, June 2003.
- [4] T. Shimizu, M. Hirakata, T. Kamezawa, and H. Watanabe, "Generation control circuit for photovoltaic modules," *IEEE Transactions on Power Electronics*, vol. 16, pp. 293–300, May 2001.
- [5] G. R. Walker and P. C. Sernia, "Cascaded dc-dc converter connection of photovoltaic modules," *IEEE Transactions on Power Electronics*, vol. 19, no. 4, pp. 1130–1139, 2004.
- [6] L. Linares, R. W. Erickson, S. MacAlpine, and M. Brandemuehl, "Improved energy capture in series string photovoltaics via smart distributed power electronics," in *Proc. Twenty-Fourth Annual IEEE Applied Power Electronics Conf. and Exposition APEC 2009*, pp. 904–910, 2009.
- [7] M. D. Seeman and S. R. Sanders, "Analysis and optimization of switched-capacitor dc-dc converters," *IEEE Transactions on Power Electronics*, vol. 23, no. 2, pp. 841–851, 2008.
- [8] J. Stauth, M. Seeman, and K. Kesarwani, "A high-voltage CMOS IC and embedded system for distributed photovoltaic energy optimization with over 99% effective conversion efficiency and insertion loss below 0.1%," in *IEEE International Solid-State Circuits Conference*, 2012.
- [9] R. C. N. Pilawa-Podgurski, *Architectures and Circuits for Low-Voltage Energy Conversion and Applications in Renewable Energy and Power Management*. PhD thesis, Department of Electrical Engineering and Computer Science Massachusetts Institute of Technology, 2012.
- [10] R. C. N. Pilawa-Podgurski, N. A. Pallo, W. R. Chan, D. J. Perreault, and I. L. Celanovic, "Low-power maximum power point tracker with digital control for thermophotovoltaic generators," in *Proc. Twenty-Fifth Annual IEEE Applied Power Electronics Conf. and Exposition (APEC)*, pp. 961–967, 2010.
- [11] D. Perreault, J. Selders, R.L., and J. Kassakian, "Frequency-based current-sharing techniques for paralleled power converters," *IEEE Transactions on Power Electronics*, vol. 13, no. 4, pp. 626–634, 1998.
- [12] D. Perreault, K. Sato, J. Selders, R.L., and J. Kassakian, "Switching-ripple-based current sharing for paralleled power converters," *IEEE Transactions on Circuits and Systems—Part I: Fundamental Theory and Applications*, vol. 46, no. 10, pp. 1264–1274, 1999.
- [13] E. Roman, R. Alonso, P. Ibanez, S. Elorduizapatarietxe, and D. Goitia, "Intelligent PV module for grid-connected PV systems," *IEEE Transactions on Industrial Electronics*, vol. 53, pp. 1066–1073, June 2006.
- [14] G. Barbose, N. Darghouth, R. Wiser, and J. Seel, "Tracking the sun IV - a historical summary of the installed cost of photovoltaics in the united states from 1998 to 2010," tech. rep., Lawrence Berkeley National Laboratory, 2011.